

## $[\alpha/\text{Fe}]$ ABUNDANCES OF FOUR OUTER M31 HALO STARS

LUIS C. VARGAS<sup>1</sup>, KAROLINE M. GILBERT<sup>2</sup>, MARLA GEHA<sup>1</sup>, ERIK J. TOLLERUD<sup>1†</sup>, EVAN N. KIRBY<sup>3</sup>, AND PURAGRA GUHATHAKURTA<sup>4</sup>

<sup>1</sup>Department of Astronomy, Yale University, 260 Whitney Ave., New Haven, CT 06511, USA; luis.vargas@yale.edu

<sup>2</sup>Space Telescope Science Institute, 3700 San Martin Dr., Baltimore, MD 21218, USA

<sup>3</sup>California Institute of Technology, 1200 E. California Blvd., MC 249-17, Pasadena, CA 91125, USA

<sup>4</sup>UCO/Lick Observatory and Department of Astronomy and Astrophysics, University of California, 1156 High St., Santa Cruz, CA 95064, USA

*Draft version March 25, 2021*

### ABSTRACT

We present alpha element to iron abundance ratios,  $[\alpha/\text{Fe}]$ , for four stars in the outer stellar halo of the Andromeda Galaxy (M31). The stars were identified as high-likelihood field halo stars by Gilbert et al. (2012) and lie at projected distances between 70 and 140 kpc from M31's center. These are the first alpha abundances measured for a halo star in a galaxy beyond the Milky Way. The stars range in metallicity between  $[\text{Fe}/\text{H}] = -2.2$  and  $[\text{Fe}/\text{H}] = -1.4$ . The sample's average  $[\alpha/\text{Fe}]$  ratio is  $+0.20 \pm 0.20$ . The best-fit average value is elevated above solar which is consistent with rapid chemical enrichment from Type II supernovae. The mean  $[\alpha/\text{Fe}]$  ratio of our M31 outer halo sample agrees (within the uncertainties) with that of Milky Way inner/outer halo stars that have a comparable range of  $[\text{Fe}/\text{H}]$ .

*Subject headings:* galaxies: abundances — galaxies: individual (M31) — galaxies: evolution — Local Group

### 1. INTRODUCTION

The assembly of galactic stellar halos via accretion of substructure is the defining feature of hierarchical galaxy formation (e.g., Searle & Zinn 1978; White & Rees 1978). Stellar halos provide a direct link between the present-day properties of a galaxy and the properties of its cosmological progenitors. In this *Letter*, we focus on chemical abundances of stellar halos to investigate this connection for M31.

Galaxy-scale  $\Lambda$ CDM simulations suggest that the accretion process deposits halo stars at all galactocentric distances (Johnston et al. 2008; Cooper et al. 2010). In the inner halo, an additional component formed in-situ adds to the complexity of stellar halos (Tissera et al. 2012; Zolotov et al. 2012). In contrast, the outer regions of halos ( $R \gtrsim 20$  kpc) are exclusively formed by accretion; stars in the outer halo encode both properties of the halo's progenitors and when they were accreted (Johnston et al. 2008; Cooper et al. 2010).

We focus here on the alpha to iron abundance ratio,  $[\alpha/\text{Fe}]$ <sup>1</sup>, of halo stars. Higher  $[\alpha/\text{Fe}]$  values are positively correlated with high star-formation rates and/or short star formation histories (Tinsley 1979). Higher  $[\alpha/\text{Fe}]$  indicates a galaxy's metal enrichment is dominated by alpha element-rich Type II supernovae (SNe), which have relatively short-lived progenitors, while later Type I SNe gradually lower  $[\alpha/\text{Fe}]$  by depositing iron into the ISM (e.g., Woosley & Weaver 1995; Nomoto et al. 2006). Hence, determining  $[\alpha/\text{Fe}]$  for outer halo stars constrains the star formation histories of the halo's progenitors.

The Milky Way (MW) halo has been investigated

with these ideas in mind. It is composed of mostly metal-poor (i.e., low  $[\text{Fe}/\text{H}]$ ) stars (Ivezić et al. 2008; Carollo et al. 2010) with elevated  $[\alpha/\text{Fe}] \sim +0.3$  abundance ratios (e.g., Fulbright 2000; Cayrel et al. 2004; Cohen et al. 2004). While most abundance measurements target nearby and thus inner halo stars, kinematical criteria have been used to identify outer halo stars passing through the inner halo for chemical abundances analysis. One exception is the study by Lai et al. (2009), who measured alpha abundances for a single star in the outer halo with a Galactocentric distance of  $\sim 40$  kpc. At the low metallicities characteristic of the outer halo ( $[\text{Fe}/\text{H}] \lesssim -2$ ; Carollo et al. 2010), the stellar population also appears to be enhanced in  $[\alpha/\text{Fe}]$  (e.g., Roederer 2009; Ishigaki et al. 2012). This pattern is different from that of present day MW satellites, which have a significant fraction of low alpha abundance ratios ( $[\alpha/\text{Fe}] \lesssim 0$ ) at  $[\text{Fe}/\text{H}] \gtrsim -2$ . Thus,  $[\alpha/\text{Fe}]$  measurements suggest that stellar halo build-up was dominated by substructure with a chemical enrichment history different from the present day MW dwarf satellites.

Simulations show a wide range in the accretion characteristics of different halos (Johnston et al. 2008; Cooper et al. 2010), motivating observational studies beyond the Galaxy. The M31 system is the nearest massive galaxy and provides hints of a quite different formation history relative to the MW. It hosts more satellite galaxies than the MW (Martin et al. 2013), with a wider range of chemical abundances (Ho et al. 2014; Vargas et al. 2014, hereafter V14). M31's halo lacks a characteristic density break (Ibata et al. 2014; Gilbert et al. 2012, hereafter G12), which suggests an extended accretion history (Deason et al. 2013). It also peaks at a  $[\text{Fe}/\text{H}]$  value  $> 1$  dex higher than the MW, qualitatively consistent with a larger fraction of halo stars coming from more luminous (and hence more metal-rich) satellites.

<sup>†</sup> Hubble Fellow

<sup>1</sup> We adopt the definition of  $[\alpha/\text{Fe}]$  as the unweighted average of  $[\text{Mg}/\text{Fe}]$ ,  $[\text{Si}/\text{Fe}]$ ,  $[\text{Ca}/\text{Fe}]$ , and  $[\text{Ti}/\text{Fe}]$ .

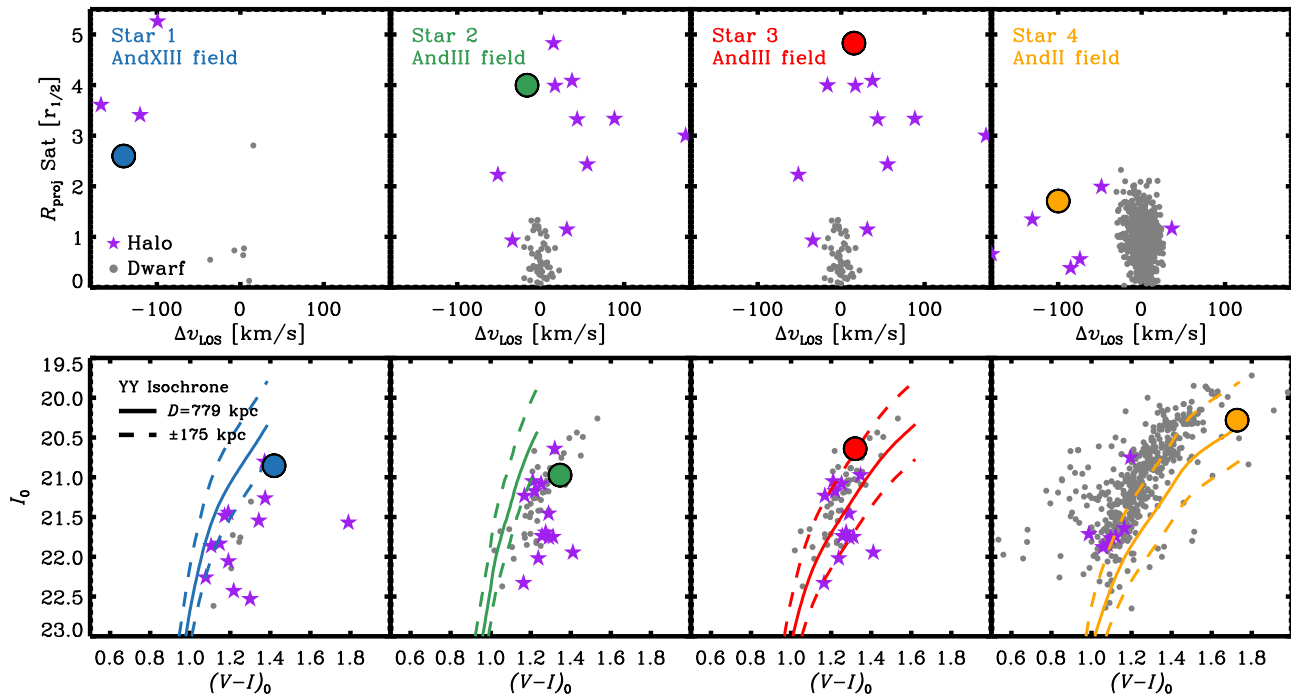


FIG. 1.— *Top*: Velocity separation,  $\Delta v_{\text{LOS}}$ , versus projected radius,  $R_{\text{proj}}$ , for each of the four field halo stars analyzed in this paper compared to the satellite galaxy located in its vicinity. Program stars are shown as large circles, and the same color coding is used throughout the paper. Other high-likelihood halo members from G12 are shown as purple stars. Satellite member stars (small grey circles) cluster at  $(\Delta v, R_{\text{proj}}) \sim (0, 0)$ . *Bottom*:  $(V - I_0, I_0)$  CMD showing the same stars as in the top panels. We overlay 12 Gyr Yale-Yonsei isochrones (Kim et al. 2002) with  $[\text{Fe}/\text{H}]$  and  $[\alpha/\text{Fe}]$  nearest to that measured spectroscopically for each of the program stars. We place the isochrones at the line-of-sight distance to M31 (solid lines) and at distances  $\pm 175$  kpc smaller/larger (dashed lines).

The metallicity-driven differences between the MW and M31 are less clear in their outer stellar halos, however, because the average stellar metallicity of M31 decreases with projected radius out to more than 100 kpc (Kalirai et al. 2006; Koch et al. 2008; Ibata et al. 2014; Gilbert et al. 2014). This suggests an underlying variation in metallicity of the progenitors of the M31 stellar halo and calls for additional chemical probes beyond  $[\text{Fe}/\text{H}]$ . However, stellar abundances other than  $[\text{Fe}/\text{H}]$  in the M31 system have so far been limited to young supergiants in the disk (Venn et al. 2000; Trundle et al. 2002). This *Letter* presents the first  $[\alpha/\text{Fe}]$  ratios measured in M31’s stellar halo.

## 2. ASSEMBLING THE SAMPLE

### 2.1. Gilbert et al. (2012)’s Halo Membership

G12 identified over 1600 M31 halo stars as part of the Spectroscopic and Photometric Landscape of Andromeda’s Stellar Halo (SPLASH) survey. They used a combination of five diagnostics to calculate the relative likelihood of membership in the M31 halo versus a foreground MW population (Gilbert et al. 2006). These diagnostics utilize photometric and spectroscopic measurements: the star’s radial velocity, its position in a  $(V - I, I)$  color-magnitude diagram (CMD), its magnitude in the narrow-band DDO51 filter, the strength of the Na I absorption line at 8190 Å and the difference between photometric and calcium triplet (CaT)-based metallicities. Stars are designated as M31 stars if it is more probable they are red giant branch (RGB) stars at the distance of M31 than MW foreground stars. Stars

are designated to have a high likelihood of M31 membership if it is 3 times more likely that they are M31 RGB stars rather than MW stars. In Section 2.3, we additionally assess whether the stars are M31 halo or M31 dwarf satellite members.

### 2.2. Higher S/N Observations

To measure metallicities and alpha abundances, we obtained higher S/N spectra of halo stars from the sample described in Section 2.1. The targets were selected due to their relative proximity to various M31 satellites studied by V14, enabling us to observe them using the multi-object masks designed for the satellite targets.

The Keck/DEIMOS spectra span the wavelength range  $6300 < \lambda < 9100$  Å and have a resolving power of  $\lambda/\Delta\lambda \sim 6000$ . The data reduction for the additional spectra follows that of the G12 sample, and was performed with a modified version of the spec2d/DEEP pipeline (Cooper et al. 2012; Newman et al. 2013) adapted to stellar spectra (Simon & Geha 2007; Kalirai et al. 2010).

Including the new observations, we identified ten likely M31 halo star with sufficient S/N ( $\gtrsim 15 \text{ \AA}^{-1}$ ) for chemical abundance analysis. Four of these candidates have a high likelihood of being M31 halo stars (Section 2.1). The other six stars are marginally identified as M31 halo stars. The likelihood distributions of MW foreground stars and M31 halo stars overlap, and the number of MW foreground stars in the sample is large at the distances from M31’s center considered here (Figure 3 of G12). Therefore, we expect contamination from MW

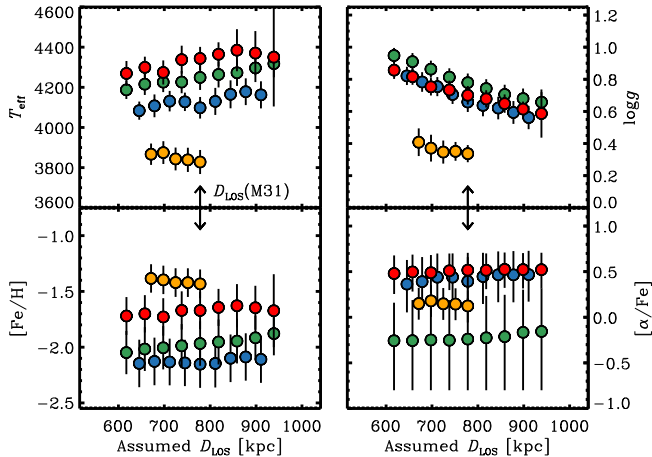


FIG. 2.— Variation of  $T_{\text{eff}}$ ,  $\log g$ ,  $[\text{Fe}/\text{H}]$ , and  $[\alpha/\text{Fe}]$  for a range of assumed line-of-sight distances, using the colors in Figure 1. The arrows mark the distance to M31. The yellow star is not plotted for  $D_{\text{LOS}} > 780$  kpc as at those distances it would be brighter than the tip of the RGB. See Section 3.2 for further discussion.

foreground stars among the stars that are marginally identified as M31 stars. For these reasons, we restrict our sample to the four high likelihood M31 members.

### 2.3. Characteristics of the Halo Sample

The four stars in our sample are located at projected distances from M31’s center of  $R_{\text{proj}} \sim 70$  to 140 kpc. At these distances, the contribution from an in-situ halo component is expected to be negligible. Instead, the halo should be dominated by metal-poor stars belonging to an accreted component (Zolotov et al. 2012).

Due to the proximity of the sample stars to various M31 satellites, we check whether our stars could be members of the nearby satellites. In the top panels of Figure 1, we plot the relative location in position-velocity space between each program halo star and the nearest satellite. The plots also include other high-likelihood halo stars (G12) as well as satellite member stars (Ho et al. 2012; Tollerud et al. 2012). The halo stars fall far from the locus of satellite member stars. In the bottom panels, we show CMDs for the same data as in the top row. Due to the similar line-of-sight distances to M31 and the satellites, CMDs are not a good discriminant of halo versus satellite membership.

## 3. CHEMICAL ABUNDANCE ANALYSIS

For the four M31 halo stars above, we measure iron abundances,  $[\text{Fe}/\text{H}]$ , and alpha to iron abundance ratios,  $[\alpha/\text{Fe}]$ , by comparing each DEIMOS spectrum to a large grid of synthetic spectral models (Kirby 2011). The technique has been applied to the study of MW satellites (Kirby et al. 2011; Vargas et al. 2013) and M31 satellites (V14). We focus on those aspects most pertinent to this work, and refer the reader to V14 for a detailed method description.

### 3.1. Measuring $[\text{Fe}/\text{H}]$ and $[\alpha/\text{Fe}]$

To find the best-fitting synthetic model, we use wavelength regions sensitive to Fe or alpha elements (here Mg, Si, Ca and Ti) and minimize the  $\chi^2$  flux difference between the spectrum and the grid models. The synthetic grid samples a wide range of  $T_{\text{eff}}$ ,  $\log g$ ,  $[\text{Fe}/\text{H}]$  and

$[\alpha/\text{Fe}]$ . After measuring the best-fitting abundances, we apply a correction factor to  $[\alpha/\text{Fe}]$  derived by V14 so that  $[\alpha/\text{Fe}]$  better represents an unweighted average of  $[\text{Mg}/\text{Fe}]$ ,  $[\text{Si}/\text{Fe}]$ ,  $[\text{Ca}/\text{Fe}]$ , and  $[\text{Ti}/\text{Fe}]$ .

Due to the large distance to M31, our spectra have relatively low S/N. Using synthetic spectra, V14 confirmed that our method can measure both alpha-solar ( $\sim +0.0$ ) and alpha-rich ( $\sim +0.4$ ) values in luminous RGB stars using  $S/N \gtrsim 15 \text{ \AA}^{-1}$  spectra with more than 93% completeness (see Figure 3 of V14).

### 3.2. Lack of Distances to M31 Halo Stars

In V14, we fixed  $\log g$  from the best color and magnitude fit to isochrones shifted to the line-of-sight distance,  $D_{\text{LOS}}$ , of each galaxy. For field halo stars,  $D_{\text{LOS}}$  is loosely constrained by the assumption that the stars lie within the M31 stellar halo. To test the change of abundance with assumed distance, we perform the abundance analysis independently for nine assumed distances, ranging between  $D_{\text{M31}} \pm \Delta D$  (see lower panels of Figure 1).  $D_{\text{M31}}$  is the distance to M31 (779 kpc; Conn et al. 2012), and  $\Delta D$  is the line-of-sight distance between M31 and the outskirts of the stellar halo at the projected distance to each star from M31. We assume a spherical stellar halo<sup>2</sup> with radius  $R_{\text{halo}} = 175$  kpc, equal to the projected distance to M31 of the most distant halo stars securely identified by G12.

We show the results of this test in Figure 2. The top panels show the variation in  $T_{\text{eff}}$  and  $\log g$  with assumed  $D_{\text{LOS}}$ . For larger  $D_{\text{LOS}}$ ,  $T_{\text{eff}}$  tends to increase (slightly) while  $\log g$  decreases. The lack of significant variation in  $T_{\text{eff}}$  is due to the primary dependence of  $T_{\text{eff}}$  on color and not on luminosity. The variation in  $\log g$  is due to the star occupying a higher-luminosity position in the CMD for larger assumed  $D_{\text{LOS}}$ . For the yellow star, stellar parameters are only shown for  $D_{\text{LOS}} \leq D_{\text{M31}}$ ; for larger  $D_{\text{LOS}}$ , the star lies above all isochrones, and would instead have to be considered a TP-AGB star. The number of TP-AGB stars is highly model dependent, but observations with large AGB samples suggest that for low metallicity systems, the fraction of TP-AGB relative to RGB stars is less than a few percent (Girardi et al. 2010). Thus, we suggest that it is improbable that this star is a TP-AGB member.

The bottom two panels show how changes in  $D_{\text{LOS}}$  translate to changes in  $[\text{Fe}/\text{H}]$  and  $[\alpha/\text{Fe}]$ . All abundance measurements vary by less than  $\sim 0.15$  dex, a change equal or smaller than all  $1\sigma$  measurement uncertainties. We note that due to the centrally concentrated M31 halo it is most likely that each star will have a line-of-sight distance similar to that of M31.

Another source of uncertainty is stellar age, since stellar parameters are measured using a grid of 12 Gyr isochrones. We test for the dependence on isochrone age by using younger, 4 Gyr isochrones. The changes in  $[\text{Fe}/\text{H}]$  and  $[\alpha/\text{Fe}]$  are  $-0.02$  and  $-0.06$  dex, respectively, lower than our minimum measurement uncertainties. Given the lack of significant change in abundances, we assume  $D_{\text{LOS}} = D_{\text{M31}}$ , and use only 12 Gyr old isochrones for the analysis below.

<sup>2</sup> The shape of the halo may deviate from sphericity in its inner regions, but all of our stars are at least 70 kpc away from M31.

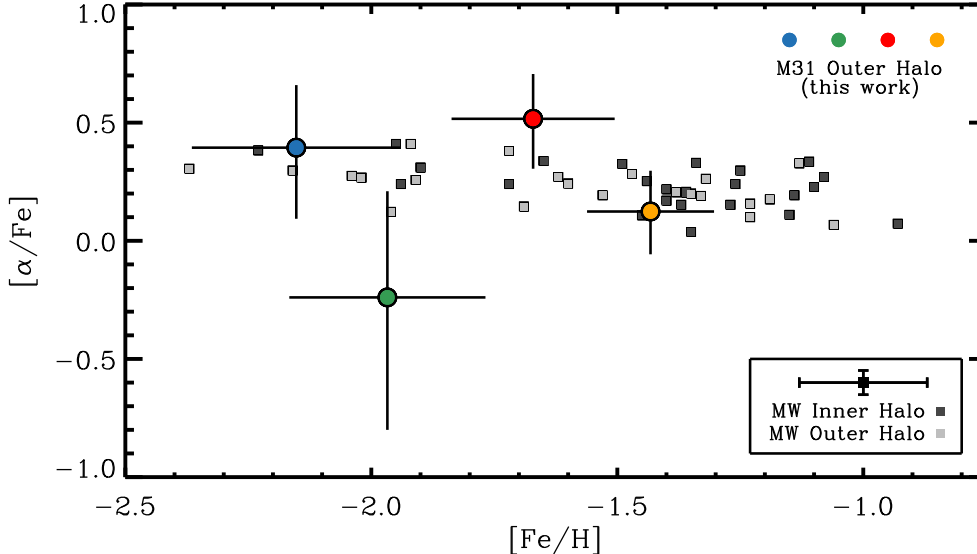


FIG. 3.—  $[\alpha/\text{Fe}]$  as a function of  $[\text{Fe}/\text{H}]$  for the four M31 halo stars. Small squares indicate MW inner/outer halo stars measured with high resolution by Ishigaki et al. (2012). A representative error bar for the MW halo measurements is included in the legend. The M31 halo stars are alpha-enhanced on average, similar to that in Milky Way halo stars of comparable metallicities.

#### 4. RESULTS

We have measured  $[\text{Fe}/\text{H}]$  and  $[\alpha/\text{Fe}]$  for four outer halo stars of M31 spanning  $\sim 1$  dex in  $[\text{Fe}/\text{H}]$ . We measure  $[\text{Fe}/\text{H}] = -2.15 \pm 0.21$ ,  $-1.97 \pm 0.20$ ,  $-1.67 \pm 0.17$ ,  $-1.43 \pm 0.13$ ; and  $[\alpha/\text{Fe}] = +0.39^{+0.26}_{-0.30}$ ,  $-0.23^{+0.45}_{-0.56}$ ,  $+0.52^{+0.19}_{-0.21}$ ,  $+0.12^{+0.17}_{-0.18}$ . The stars are located between  $R_{\text{proj}} \sim 70$  and 140 kpc from M31. In Figure 3 we plot our  $[\text{Fe}/\text{H}]$  and  $[\alpha/\text{Fe}]$  measurements. Three out of the four stars have  $[\alpha/\text{Fe}] > 0.0$ , consistent with typical MW halo values within the uncertainties (see Section 4.1). While the fourth star has  $[\alpha/\text{Fe}] < 0$ , its large uncertainty does not allow us to distinguish whether it is drawn from an alpha-poor population enriched by Fe-rich Type Ia SNe, or is an  $[\alpha/\text{Fe}]$  enhanced star scattered to low  $[\alpha/\text{Fe}]$ . Low  $[\alpha/\text{Fe}]$  and  $[\text{Fe}/\text{H}]$  stars have been detected in the MW halo but are rare (Ivans et al. 2003). Our sample is too small to detect an intrinsic range in  $[\alpha/\text{Fe}]$  in the M31 halo.

##### 4.1. Average $[\alpha/\text{Fe}]$ in the M31 Outer Halo and Comparison to Milky Way

To draw conclusions from our small sample, we determine the sample average  $[\alpha/\text{Fe}]$  ratio in two ways. First, we measure the unweighted average and its uncertainty taking into account the small sample size from the Student- $t$  distribution. We obtain  $\langle [\alpha/\text{Fe}] \rangle = +0.20 \pm 0.20$ . An inverse-variance weighted mean yields  $\langle [\alpha/\text{Fe}] \rangle = +0.28 \pm 0.12$ , but Monte Carlo tests by V14 suggest that this weighting could bias the average high by  $\sim +0.05 - 0.10$  due to a modest anti-correlation between  $[\alpha/\text{Fe}]$  and its uncertainty. Second, we recalculate  $\langle [\alpha/\text{Fe}] \rangle$  by weighting our measurements by their expected fractional contribution to the halo from Gilbert et al. (2014)’s metallicity distribution function (MDF), shown in Figure 4. We use the thicker histogram, corresponding to stars at the same projected distances from M31 as our stars. We draw 10,000 realizations of  $[\text{Fe}/\text{H}]$  and  $[\alpha/\text{Fe}]$  from each of our four stars using their best-fit values and individual errors. Each re-

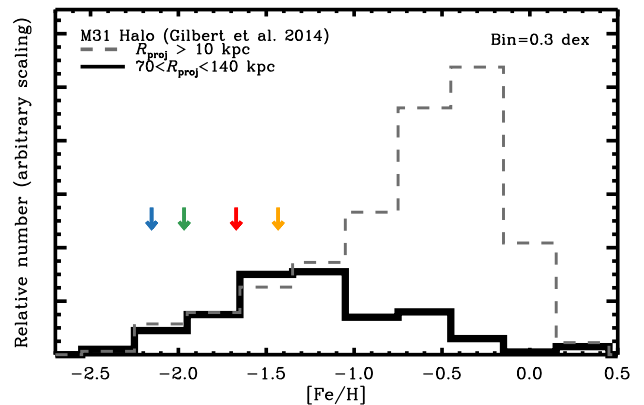


FIG. 4.— MDF for M31 outer halo stars in the same range of distances as our  $[\alpha/\text{Fe}]$  sample (solid histogram), and for halo stars at all distances (thin dashed histogram), using the photometric metallicities from G14. The bin size is equal to the mean  $[\text{Fe}/\text{H}]$  uncertainty for metal-poor stars in the MDF ( $= \sigma \sim 0.29$ ). The y-axis is scaled arbitrarily to show the shapes of the two histograms. The four stars presented in this paper span roughly the metal-poor half of the outer halo MDF.

alization is thus a sample of four  $([\text{Fe}/\text{H}], [\alpha/\text{Fe}])$  pairs. We reorder the pairs by  $[\text{Fe}/\text{H}]$  and calculate weights for each  $[\alpha/\text{Fe}]$  value as the area under the normalized MDF bounded by the midpoint between the  $[\text{Fe}/\text{H}]$  value of each of our data points and the previous/next value. We truncate the MDF to the range of  $[\text{Fe}/\text{H}]$  abundances of our stars. From the 10,000 realizations, we measure  $\langle [\alpha/\text{Fe}] \rangle = +0.19 \pm 0.14$ , in agreement with the simple average.

We next compare  $[\alpha/\text{Fe}]$  between the MW and M31 halos. For the MW, we use the homogeneous sample by Ishigaki et al. (2012), who classify stars as inner or outer halo stars kinematically. We select all 68 stars with reported measurements of  $[\text{Mg}/\text{Fe}]$ ,  $[\text{Si}/\text{Fe}]$ ,  $[\text{Ca}/\text{Fe}]$ , and  $[\text{Ti}/\text{Fe}]$  to calculate  $[\alpha/\text{Fe}]$  consistently with our own definition of  $[\alpha/\text{Fe}]$  (see Section 3.1). The MW points are also plotted in Figure 3. We calculate  $\langle [\alpha/\text{Fe}] \rangle$  for

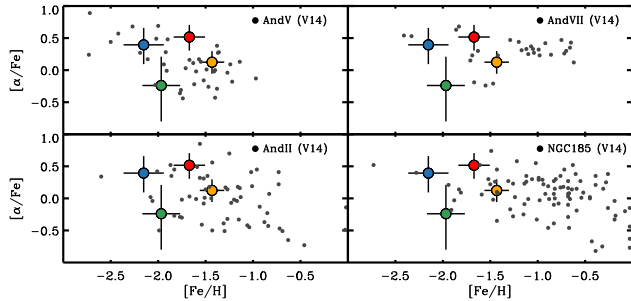


FIG. 5.— Comparison of the four field halo star  $[\alpha/\text{Fe}]$  abundances with those of the four M31 satellites with the largest number of measurements (V14, small circles). Both halo and satellite samples come from DEIMOS spectra of RGBs with similar S/N, analyzed with the same method. The halo sample is more metal-poor than the two brighter satellites.

both MW inner and outer halo subsamples, finding unweighted averages of  $\langle[\alpha/\text{Fe}]\rangle = +0.23$  in both cases. Thus, our average  $[\alpha/\text{Fe}]$  value for M31’s outer halo stars ( $\langle[\alpha/\text{Fe}]\rangle = 0.20 \pm 0.20$ ) is consistent with the MW value within the uncertainties (in the same range of metallicities).

#### 4.2. M31 Halo versus Satellite Galaxies

The lower  $[\alpha/\text{Fe}]$  ratios in MW surviving satellites relative to MW halo stars (e.g., Venn et al. 2004; Kirby et al. 2011) have been used to infer that MW halo progenitors had short-lived and rapid star formation histories relative to the surviving satellites (Robertson et al. 2005). Using our sample and V14, we compare in Figure 5 the alpha abundances between the halo and the four present-day M31 satellites with the largest samples (And V, And VII, And II, and NGC 185). The satellites range in luminosity from  $7 \times 10^5 L_{\odot}$  (And V) to  $1.8 \times 10^8 L_{\odot}$  (NGC 185). Thus, they sample a wide range of the satellite luminosity function except for the faint end.

The average  $[\text{Fe}/\text{H}]$  of our halo sample is most similar to those of the less luminous And V and And VII, whereas And II and NGC 185 are more metal-rich. Our small sample size precludes strong statistical comparisons between halo and satellite abundances, but we make a first attempt by comparing  $\langle[\alpha/\text{Fe}]\rangle$ . V14 measured average  $[\alpha/\text{Fe}]$  ratios of  $0.12 \pm 0.09$ ,  $0.30 \pm 0.09$ ,  $0.03 \pm 0.09$  and  $0.12 \pm 0.09$  for And V, And VII, And II, and NGC185, respectively. Thus, none of the satellites have an  $\langle[\alpha/\text{Fe}]\rangle$  value discrepant by more than  $1\sigma$  from the halo value calculated in Section 4.1,  $\langle[\alpha/\text{Fe}]\rangle = +0.20 \pm 0.20$ . The comparison between the halo and satellites must thus be revisited with larger samples.

## 5. DISCUSSION AND CONCLUSIONS

We present the first  $[\alpha/\text{Fe}]$  measurements of stars in a stellar halo beyond the MW. The average  $[\alpha/\text{Fe}]$  of our four M31 outer halo stars is  $0.20 \pm 0.20$ . The metallicities of the four stars sample roughly the metal-poor half of the metallicity distribution of the outer halo at distances comparable to those of our four stars ( $70 \lesssim R_{\text{proj}} \lesssim 140$  kpc).

High alpha enhancements are characteristic of Type II SNe enrichment of the ISM operating on short timescales. Thus, the best-fit high average  $[\alpha/\text{Fe}]$  ratio in the outer M31 halo combined with the low halo metallicity at these projected distances hints towards a progenitor population that came into proximity with the proto-M31 halo at early times. In simulations of halo formation, dwarf satellites with high  $\langle[\alpha/\text{Fe}]\rangle$  and low  $\langle[\text{Fe}/\text{H}]\rangle$  correlate with elevated star formation rates, early accretion, (Johnston et al. 2008; Tissera et al. 2012) and/or were more affected by gravitational tidal interactions (Nichols et al. 2014). An alternate pathway for producing a high  $[\alpha/\text{Fe}]$  population is to invoke the dissolution of globular clusters. In the MW halo, globular clusters may have contributed anywhere from a few to 50% of the halo stellar mass (e.g., Carretta et al. 2010; Martell et al. 2011). Given the  $[\alpha/\text{Fe}]$  enhancements of present-day M31 globular clusters ( $\langle[\alpha/\text{Fe}]\rangle = +0.37 \pm 0.16$ , Colucci et al. 2009), this formation pathway may also hold in the M31 halo.

The M31 halo enrichment pattern agrees with that of the MW halo, whether considering inner or outer halo stars. Given the apparent differences in accretion histories between the MW and M31 stellar halos, it is somewhat surprising that both share similar chemical properties (at similar metallicities). More measurements of  $[\alpha/\text{Fe}]$  in outer halo stars of the MW and M31 are needed to better compare the chemical properties of the principal progenitors of both outer halos.

#### ACKNOWLEDGEMENTS

LCV acknowledges useful conversations with Nikhil Padmanabhan during the analysis stage of this project. LCV was supported by the National Science Foundation Graduate Research Fellowship (Grant No. DGE-1122492). MG and LCV acknowledge support from NSF Grant AST-0908752, and PG acknowledges support from NSF grant AST-1010039. EJT and KG were supported by NASA through Hubble Fellowship Grant Nos. 51316.01 and 51273.01, awarded by the Space Telescope Science Institute, which is operated by the Association of Universities for Research in Astronomy, Inc., for NASA, under contract NAS 5-26555. *Facilities:* Keck II (DEIMOS)

#### REFERENCES

- Carollo, D., Beers, T. C., Chiba, M., et al. 2010, *ApJ*, 712, 692  
 Carretta, E., Bragaglia, A., Gratton, R. G., et al. 2010, *A&A*, 516, A55  
 Cayrel, R., Depagne, E., Spite, M., et al. 2004, *A&A*, 416, 1117  
 Cohen, J. G., Christlieb, N., McWilliam, A., et al. 2004, *ApJ*, 612, 1107  
 Colucci, J. E., Bernstein, R. A., Cameron, S., McWilliam, A., & Cohen, J. G. 2009, *ApJ*, 704, 385  
 Conn, A. R., Ibata, R. A., Lewis, G. F., et al. 2012, *ApJ*, 758, 11  
 Cooper, A. P., Cole, S., Frenk, C. S., et al. 2010, *MNRAS*, 406, 744  
 Cooper, M. C., Newman, J. A., Davis, M., Finkbeiner, D. P., & Gerke, B. F. 2012, *spec2d: DEEP2 DEIMOS Spectral Pipeline*, astrophysics Source Code Library  
 Deason, A. J., Belokurov, V., Evans, N. W., & Johnston, K. V. 2013, *ApJ*, 763, 113  
 Font, A. S., Johnston, K. V., Bullock, J. S., & Robertson, B. E. 2006, *ApJ*, 638, 585  
 Fulbright, J. P. 2000, *AJ*, 120, 1841  
 Gilbert, K. M., Guhathakurta, P., Kalirai, J. S., et al. 2006, *ApJ*, 652, 1188

- Gilbert, K. M., Guhathakurta, P., Beaton, R. L., et al. 2012, *ApJ*, 760, 76
- Gilbert, K. M., Kalirai, J. S., Guhathakurta, P., et al. 2014, [astro-ph/1409.3843](#)
- Girardi, L., Williams, B. F., Gilbert, K. M., et al. 2010, *ApJ*, 724, 1030
- Ho, N., Geha, M., Tollerud, E., et al. 2014, [astro-ph/1405.4424](#)
- Ho, N., Geha, M., Munoz, R. R., et al. 2012, *ApJ*, 758, 124
- Ibata, R. A., Lewis, G. F., McConnachie, A. W., et al. 2014, *ApJ*, 780, 128
- Ivans, I. I., Sneden, C., James, C. R., et al. 2003, *ApJ*, 592, 906
- Ishigaki, M. N., Chiba, M., & Aoki, W. 2012, *ApJ*, 753, 64
- Ivezić, Ž., Sesar, B., Jurić, M., et al. 2008, *ApJ*, 684, 287
- Johnston, K. V., Bullock, J. S., Sharma, S., et al. 2008, *ApJ*, 689, 936
- Kalirai, J. S., Gilbert, K. M., Guhathakurta, P., et al. 2006, *ApJ*, 648, 389
- Kalirai, J. S., Beaton, R. L., Geha, M. C., et al. 2010, *ApJ*, 711, 671
- Kim, Y.-C., Demarque, P., Yi, S. K., & Alexander, D. R. 2002, *ApJS*, 143, 499
- Kirby, E. N. 2011, *PASP*, 123, 531
- Kirby, E. N., Cohen, J. G., Smith, G. H., et al. 2011, *ApJ*, 727, 79
- Koch, A., Rich, R. M., Reitzel, D. B., et al. 2008, *ApJ*, 689, 958
- Lai, D. K., Rockosi, C. M., Bolte, M., et al. 2009, *ApJ*, 697, L63
- Martell, S. L., & Grebel, E. K. 2010, *A&A*, 519, A14
- Martell, S. L., Smolinski, J. P., Beers, T. C., & Grebel, E. K. 2011, *A&A*, 534, A136
- Martin, N. F., Ibata, R. A., McConnachie, A. W., et al. 2013, *ApJ*, 776, 80
- Newman, J. A., Cooper, M. C., Davis, M., et al. 2013, *ApJS*, 208, 5
- Nichols, M., Revaz, Y., & Jablonka, P. 2014, *A&A*, 564, A112
- Nomoto, K., Tominaga, N., Umeda, H., Kobayashi, C., & Maeda, K. 2006, *Nuclear Physics A*, 777, 424
- Robertson, B., Bullock, J. S., Font, A. S., Johnston, K. V., & Hernquist, L. 2005, *ApJ*, 632, 872
- Roederer, I. U. 2009, *AJ*, 137, 272
- Searle, L., & Zinn, R. 1978, *ApJ*, 225, 357
- Simon, J. D., & Geha, M. 2007, *ApJ*, 670, 313
- Tinsley, B. M. 1979, *ApJ*, 229, 1046
- Tissera, P. B., White, S. D. M., & Scannapieco, C. 2012, *MNRAS*, 420, 255
- Tollerud, E. J., Beaton, R. L., Geha, M. C., et al. 2012, *ApJ*, 752, 45
- Trundle, C., Dufton, P. L., Lennon, D. J., Smartt, S. J., & Urbaneja, M. A. 2002, *A&A*, 395, 519
- Vargas, L. C., Geha, M., Kirby, E. N., & Simon, J. D. 2013, *ApJ*, 767, 134
- Vargas, L. C., Geha, M. C., & Tollerud, E. J. 2014, *ApJ*, 790, 73
- Venn, K. A., Irwin, M., Shetrone, M. D., et al. 2004, *AJ*, 128, 1177
- Venn, K. A., McCarthy, J. K., Lennon, D. J., et al. 2000, *ApJ*, 541, 610
- White, S. D. M., & Rees, M. J. 1978, *MNRAS*, 183, 341
- Woosley, S. E., & Weaver, T. A. 1995, *ApJS*, 101, 181
- Zolotov, A., Brooks, A. M., Willman, B., et al. 2012, *ApJ*, 761, 71